Available online at www.sciencedirect.com
ScienceDirect
Trans. Nonferrous Met. Soc. China 25(2015) 1770−1778
Transactions of Nonferrous Metals Society of China
www.tnmsc.cn

Microstructure and mechanical properties of friction stir welded AA7075−T651 aluminum alloy thick plates

T. SRINIVASA RAO[1], G. MADHUSUDHAN REDDY[2], S. R. KOTESWARA RAO[3]

1. Department of Mechanical Engineering, Tagore Engineering College, Chennai 600127, Tamil Nadu, India;
2. Metal Joining Group, Defense Metallurgical Research Laboratory, Hyderabad 500058, Telangana, India;
3. Department of Mechanical Engineering, SSN College of Engineering, Kalavakkam 603110, Tamil Nadu, India

Received 5 July 2014; accepted 20 January 2015

Abstract: Friction stir butt welding of AA7075−T651 plates with thicknesses of 10 and 16 mm was investigated. Defect-free, full-penetration welds were obtained after careful process parameter selection. While the nuggets in both welds exhibited very fine recrystallized grains, and finer grains were observed in welds made on 10 mm thick plates. Microhardness surveys revealed that significant loss in hardness occurs in the heat-affected zone. The reduction in hardness due to the welding process is higher in the case of welds made on 16 mm thick plates. Welds made on 10 mm thick plates exhibited superior tensile properties compared with those made on 16 mm thick plates. Fracture during tensile test occurred in the heat-affected zone in both cases. TEM images of specimens revealed that the heat-affected zone consisted of widened precipitate-free zones along grain boundaries and partial dissolution of precipitates in the grain interiors. It is concluded that defect-free single pass welds can be made on AA7075−T651 thick plates using friction stir welding and the welds made on 10 mm thick plates exhibit high joint efficiency.

Key words: AA7075−T651 aluminum alloy; friction stir welding; microstructure; mechanical properties

1 Introduction

High-strength, precipitation-hardening 7000 series aluminum alloys such as alloy 7075 are used extensively in aircraft primary structures. Their high specific strength, along with their natural aging characteristics, makes them appropriate for various structural applications in aerospace [1]. In recent years, there have been proposals to use high strength aluminum alloys from 7000 series, particularly the alloy AA7075, in the fabrication of heavy vehicle hulls. However, it has been clearly established that this class of aluminum alloys are generally not recommended for welding using fusion welding processes due to severe hot cracking problem [2]. After the advent of friction stir welding (FSW) in 1991 aluminum alloys that were considered unweldable were shown to be weldable using FSW, that too with very high joint efficiency [3−8].

Friction stir welding that is a solid-state process, invented at TWI, UK, is a viable technique for joining aluminum alloys [9]. To friction stir weld either a butt or lap joint, a specially designed non-consumable cylindrical tool is rotated and plunged into the joint line. The tool has a small diameter pin with a large diameter shoulder. The frictional heat generated by the welding tool makes the surrounding material softer and allows the tool to move along the joint line. The depth of penetration is controlled by the tool shoulder and the length of entry probe. When the tool shoulder touches the metal plates being joined, its rotation generates additional frictional heat that in turn plasticizes a cylindrical metal column around the plunged tool pin. The rotating tool produces a continual hot working action, plasticizing the material within a narrow zone while transferring metal to the trailing edge from the leading face of the tool pin. The FSW process generates three distinct microstructural zones: the weld nugget (WN), the thermo-mechanically-affected zone (TMAZ) and the heat-affected zone (HAZ). The WN is the region through which the tool pin passes, and thus experiences high plastic deformation and high heat. Due to recrystallization, it usually consists of fine equiaxed grains. The TMAZ adjacent to the nugget is the region where the metal is plastically deformed as well as heated, but this is not sufficient to cause recrystallization. The

Corresponding author: T. SRINIVASA RAO; Tel: +91-44-27409725; E-mail: srinutadivaka@yahoo.com
DOI: 10.1016/S1003-6326(15)63782-7

HAZ experiences only a heating effect, without any mechanical deformation.

Considerable amount of work has been reported by various researchers [10−26] highlighting the changes in microstructures due to the associated plastic deformation and frictional heat during FSW. Dissolution and coarsening of strengthening precipitates [10−12,18, 23−26] as well as the formation of wide precipitate-free zones [12,18,25] have been identified in the weld region. Investigations on mechanical failure of the welds have been carried out by several investigators [19−21] and they found that failure can take place in the WN, HAZ or TMAZ regions depending on the amount of heat input, which is usually governed by process parameters such as rotational speed and travel speed. The dependence of weld microstructure on processing parameters has also been revealed [22−24].

Most of these studies have been conducted on plates with thickness less than 10 mm, which are suitable to aerospace industry and currently FSW of aluminum alloys is widely employed in aerospace, shipping and automobile industries. Though it has been established that FSW of thick plates up to 25 mm is definitely possible with 80% joint efficiency [27], several details such as tool geometry and optimum parameters are not published. Variations in microstructures in the through thickness direction were not clearly investigated. As the thickness of the plate to be welded increases, variations in microstructures and properties can be expected which have not been widely investigated in the available literature. Thus, the objectives of this study are to evaluate the microstructural changes and mechanical properties of welds made on 10 and 16 mm thick AA7075−T651 aluminum alloy using friction stir welding.

2 Experimental

Experiments were performed on rolled plates of 10 and 16 mm thick AA7075–T651 aluminum alloys, having chemical composition as shown in Table 1. The dimensions of base metal plates were 110 mm (width) × 240 mm (length). The plates were longitudinally butt-welded using a commercially available friction stir welding machine. The process parameters used for friction stir welding are given in Table 2. These parameters were arrived at after extensive trials aiming at defect-free, full-penetration welds.

Table 1 Chemical composition of AA7075–T651 alloy (mass fraction, %)

Zn	Mg	Cu	Si	Fe	Cr	Ti	Mn	Al
6.0	2.5	1.4	0.03	0.08	0.20	0.05	0.01	Bal.

Specimens for metallographic examination were carefully sliced to the required sizes from the welded joint consisting of WN, TMAZ, HAZ and base metal regions. Emery papers of different grades were used for polishing the sliced specimens. Diamond compound (particle size of 1 μm) was used for final polishing in a disk polishing machine. The polished samples were etched using standard Keller’s reagent (5 mL HNO_3+ 2 mL HF+3 mL HCl+190 mL distilled water) to observe the microstructure of the welds. Macro and microstructural studies were carried out using a optical microscopy.

Specimens for transmission electron microscopy (TEM) were cut from various regions of the weld made on 10 mm thick plates (Fig. 1), using an electrical-discharge cutting machine. Thinning of the specimens was done by hand at a very slow pace to avoid any heat generation. Electrolytic thinning of specimens was carried out on an electro polisher in the presence of nitric acid and methanol solution. Microstructural investigation was carried out on a JEM−2100 electron microscope with EDX capabilities.

Hardness surveys were carried out using Vickers hardness testing machine, at the mid-thickness of the polished cross-sections at a spacing of 1 mm between the adjacent indentations, a load of 0.1 kg and dwell time of 10 s. Tensile specimens transverse to the weld were prepared according to ASTM B557 standard as shown in Fig. 2. Room-temperature tensile tests were carried out on a computer-controlled universal testing machine. The results of tensile tests conducted for welds produced in 10 mm (10-mm-weld) and 16 mm thick plates (16-mm-weld) are given in Table 3.

Transverse face and root bend tests were conducted

Table 2 Friction stir welding process parameters

Thickness of plate/mm	Tool geometry	Tool rotational speed/($r\cdot min^{-1}$)	Welding speed/ ($mm\cdot min^{-1}$)	Tool tilt/(°)
10	M2 tool steel; taper threaded pin (left hand metric threads, 1.5 mm pitch); pin diameter: 7 mm (shoulder end) and 4 mm (tip end); pin length: 9.5 mm; shoulder diameter: 22 mm; flat shoulder	700	120	1.5
16	M2 tool steel; taper threaded pin (left hand metric threads, 1.5 mm pitch); pin diameter: 10 mm (shoulder end) and 8 mm (tip end); pin length: 15 mm shoulder diameter: 30 mm flat shoulder	500	25	1.5

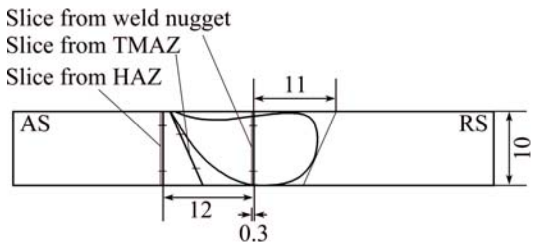

Fig. 1 Slicing of specimens for TEM studies (unit: mm)

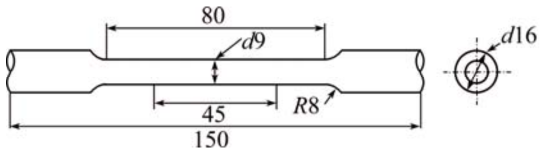

Fig. 2 Tensile test specimen dimensions for 16-mm-weld (unit: mm)

Table 3 Results of transverse tensile testing (average of three tests)

Material	Yield strength (0.2% proof)/ MPa	Ultimate tensile strength/ MPa	Elongation/ %	Joint efficiency in terms of UTS/%	Fracture location
10 mm thick base material	539	609	13	−	−
10-mm-weld	320	424	6	70	HAZ
16 mm thick base material	563	610	10	−	−
16-mm-weld	192	330	8	54	HAZ

on both 10-mm-welds and 16-mm-welds according to ASTM E190 standard. The specimen dimensions used for the test were 152 mm × 38 mm × 10 mm. Bend tests were also conducted on both 10 mm and 16 mm thick base plates. Impact specimens were prepared as per ASTM E23 standard. Impact tests were carried out on Charpy impact test machine and the results are presented in Table 4.

Table 4 Results of impact testing (average of three tests)

Material	Impact toughness/J
10 mm thick base material	6.67
10-mm-weld	4.00
16 mm thick base material	6.67
16-mm-weld	6.00

3 Results and discussion

3.1 Metallurgical investigation

Macroscopic appearances of the cross-section of the 10-mm-welds and 16-mm-welds are shown in Fig. 3. The flow and mixing are easy to be observed due to etching characteristics of the alloy. Fusion welding of aluminum alloys is naturally accompanied by various weld defects such as slag inclusion, solidification cracks and porosity which deteriorate the quality of the weld. On the other hand, friction stir welding is known to be free from defects related to solidification, since there is no melting that takes place during welding process. In FSW, metal plates are joined together due to frictional heat produced and metal flow by the stirring action.

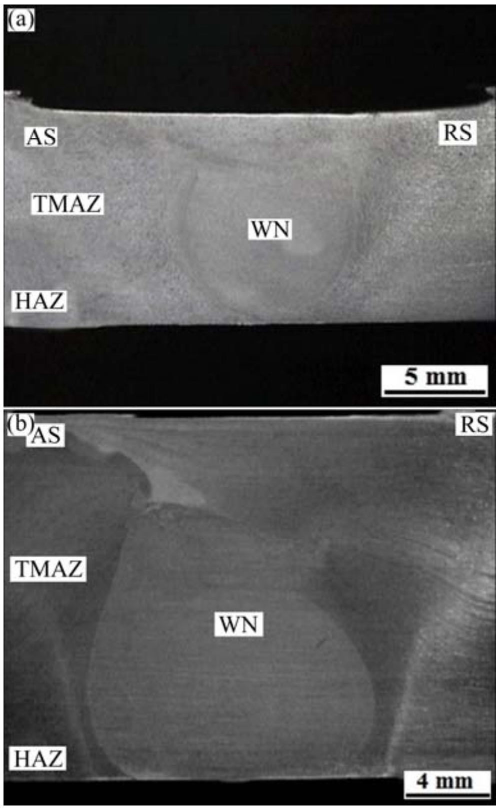

Fig. 3 Macrographs showing various microstructural zones of friction stir welds (AS: Advancing side, RS: Retreating side): (a) 10-mm-weld; (b) 16-mm-weld

However, friction stir welds are known to have other defects such as tunnel defect, cracks, and pin hole, worm hole, zig-zag line due to improper flow of metal and insufficient consolidation of metal in FSW (weld nugget) region [28]. As it can be seen, no obvious welding defect is found in both 10-mm-weld (Fig. 3(a)) and 16-mm-weld (Fig. 3(b)), indicating that sound welds are obtained. Based on the microstructural characterization of grains, three different zones such as WN, TMAZ, and HAZ have been identified. A typical macrograph showing various microstructural zones revealed the formation of onion structured weld nugget, which was considered to be a common feature in friction stir welds of aluminum alloy as the same was also reported by various investigators [11,18].

The base material microstructure consisted of large elongated pancake shaped grains typical of a hot rolled structure (Figs. 4(a) and 5(a)). TEM image of the base material reveals two populations: one group at 50−75 nm and the other group at 10−20 nm (Fig. 6(a)). There is some disagreement in the literature on the exact composition of these strengthening precipitates. WERT [29] reported these strengthening precipitates as a solid solution of isomorphous phases $MgZn_2$ and MgAlCu, which is described as $Mg(Zn_2,AlCu)$. On the other hand, LORIMER [30] reported that these are $Mg_{32}(Al,Zn)_{49}$, having BCC crystal structure. He also reported that these precipitates could be η phase ($MgZn_2$) form. Thus, the larger precipitates can be indexed as $Mg(Zn_2,AlCu)$ or $Mg_{32}(Al,Zn)_{49}$. The possibility of both types of precipitates cannot be ruled out.

In the weld nugget, for both 10-mm-welds and 16-mm-welds, the microstructure was characterized by fine and equiaxed grains (Figs. 4(b) and 5(b)). FSW process creates intense plastic deformation associated with the movement of material from the front to the back of the rotating pin. The material undergoes localized heating because of frictional effects as well as plastic deformation. RHODES et al [11] and MAHONEY et al [18] reported that temperatures reached 400−480 °C in regions adjacent to the FSW nugget during friction stir welding of the 7075 Al alloy. It is reasonable to predict that the temperature in the weld nugget itself is as hot as the highest peak temperature in adjacent regions. The frictional heating and extensive plastic deformation generate fine recrystallized equiaxed grains in the weld nugget. In this study, a fine recrystallized equiaxed grain structure was obtained in the weld nugget. The weld nugget of 10-mm-welds (Fig. 4(b)) showed finer grains (10 μm) compared with that of (20 μm) 16-mm-welds (Fig. 5(b)).

TEM micrograph of the weld nugget shows a randomly oriented intra granular precipitates of 60−80 nm in size and look to be disks or plates (Fig. 6(b)). These precipitates seem to be the same type of precipitates as the 50−75 nm particles oriented in the rolling direction in the base material. The redistribution from the orientation of rolling direction to random suggests that these particles have gone into solution and re-precipitated during the welding process. Constituent particles prevail in the weld nugget in a distribution similar to that found in the base material. There are not very fine (10 nm) intergranular precipitates in the base material. The recrystallization of the weld nugget grains and redistribution of the precipitates indicate that the

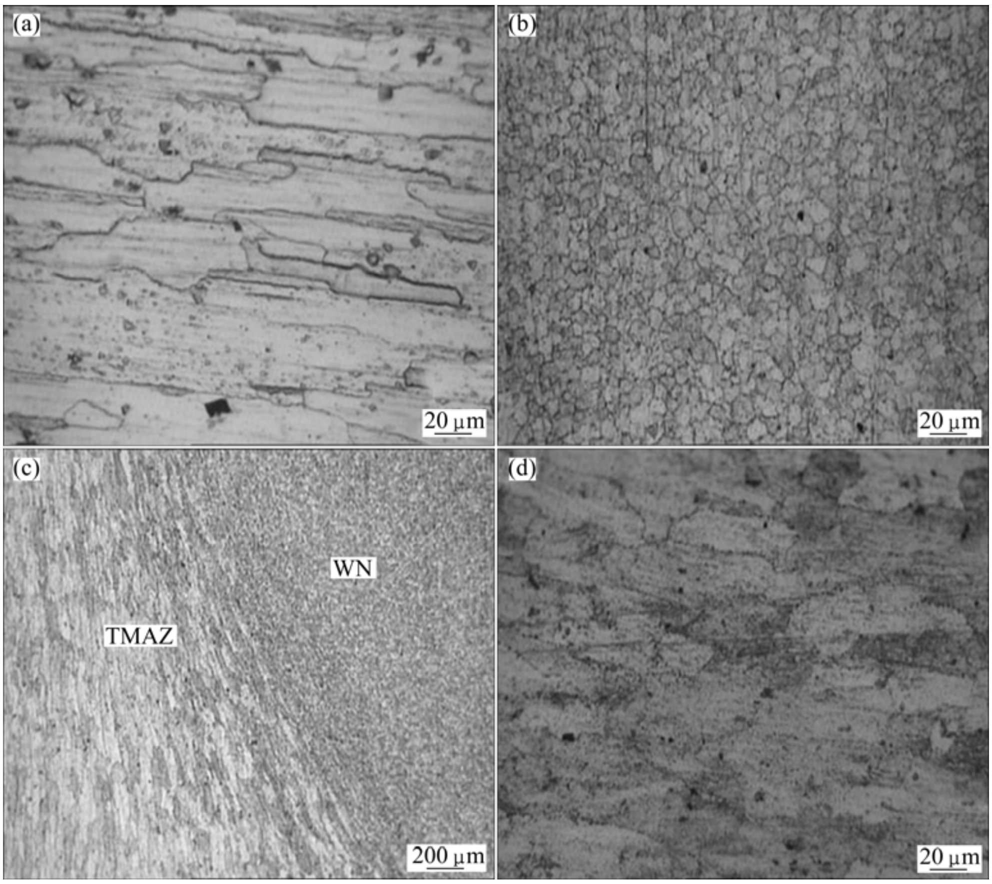

Fig. 4 Optical micrographs of 10 mm thick friction stir welded AA 7075−T651 alloy: (a) Base material; (b) Weld nugget; (c) TMAZ; (d) HAZ

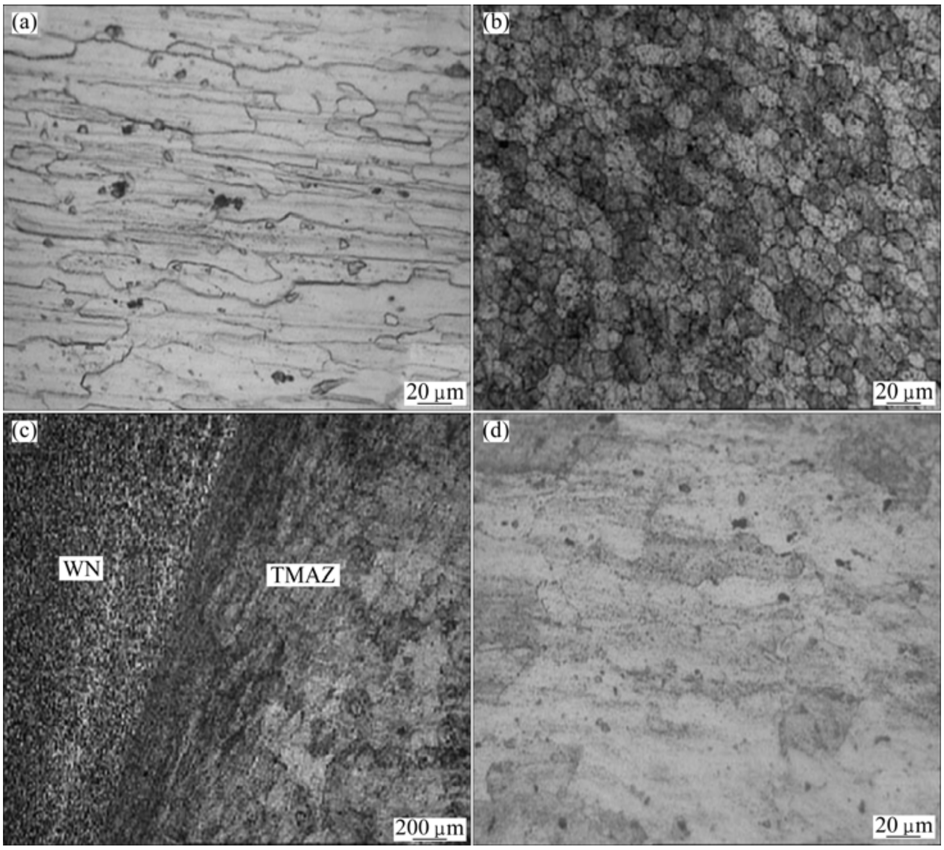

Fig. 5 Optical micrographs of 16 mm thick friction stir welded AA7075−T651 alloy: (a) Base material; (b) Weld nugget; (c) TMAZ; (d) HAZ

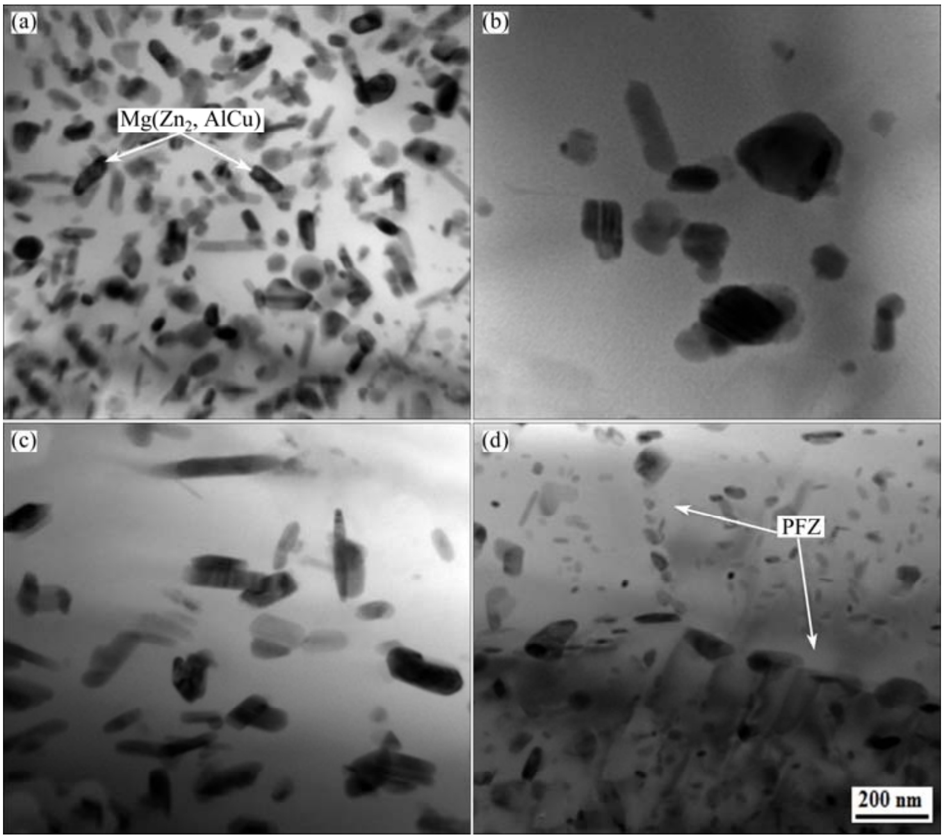

Fig. 6 TEM images of 10 mm thick friction stir welded AA7075−T651 alloys: (a) Base material; (b) Weld nugget; (c) TMAZ; (d) HAZ

temperature range during welding process is above the solution temperature for the hardening precipitates, but below the melting temperature of the alloy. A likely temperature is somewhere between 450 and 480 °C [29,30]. Apparently, the cooling rates made that the larger precipitates could nucleate and grow, but the finer ones could not nucleate, i.e., the cooling curve interacts the time−temperature transformation curve at a temperature above the nose.

The transition zone between the base material and weld nugget was characterized by a highly deformed structure both in 10-mm-welds (Fig. 4(c)) and 16-mm-welds (Fig. 5(c)). The elongated grains in base material were deformed in an upward flowing pattern around the fine grain nugget. Though there is an element of plastic deformation in the transition zone, no recrystallization occurs in this zone. Figure 6(c) shows the TEM image of the TMAZ. As it can be observed, there is no significant difference in larger hardening precipitates, either in size or morphology, during the welding process. The smaller precipitates, on the other hand, have coarsened (Fig. 6(c)).

The HAZ retained the same grain structure as the parent material both in 10-mm-welds (Fig. 4(d)) and 16-mm-welds (Fig. 5(d)). However, the thermal exposure above 250 °C exerted a significant effect on the precipitate structure. Figure 6(d) shows a representative micrograph of intragranular and grain boundary precipitates in the HAZ. Precipitates inside the grains retain homogeneous distribution. Regions surrounding grain boundaries are found to be free of precipitates, which are widely branded as precipitate free zones (or PFZs). Aluminum alloys suffer a great deal from the formation of precipitate free zones, because not only they are frequently strengthened using precipitation hardening, but also they contain high concentrations of vacancies. The PFZs are obvious regions of weakness.

3.2 Mechanical behaviour

3.2.1 Microhardness

Vickers microhardness tests were conducted across the weld at middle thickness for both 10-mm-welds and 16-mm-welds, to ascertain the possible microstructure and property variation among various zones of the weldment. The representative hardness distributions are shown in Fig. 7. As it can be seen, both the distributions exhibit “W” shaped appearance, typical of 7xxx series alloys welded under conditions for which the nugget temperature is close to the solution heat treatment temperature. The weld nugget region of 10-mm-weld exhibits hardness which is close to T6 hardness, whereas in 16-mm-weld, the weld nugget hardness is found to be HV 155 (average) though the base plates recorded approximately the same hardness value. It is observed that in case of 10-mm-welds, the lowest hardness values are higher than those observed in 16-mm-welds. Both 10-mm-weld and 16-mm-weld record the lowest hardness values in HAZ on advancing side. Loss in hardness due to the welding process is significantly higher in the case of welds made on 16 mm thick plates, mainly due to the higher heat inputs employed to obtain sound welds.

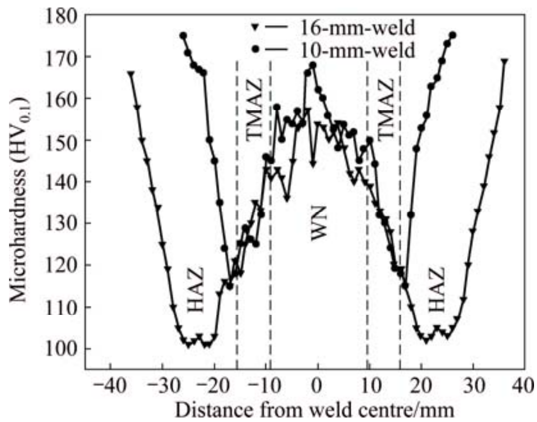

Fig. 7 Microhardness profiles of friction stir welds made on 10 mm and 16 mm thick AA7075−T651 plates

As it can be seen from Fig. 8, substantial overaging leads to the minimum hardness in the HAZ. This suggests that the tensile specimens are prone to fracture in this zone. It is shown in the next section that the strength values also vary in accordance with the hardness profiles of the welds. The enhanced hardness in the weld nugget can be attributed to finer grain size of the weld nugget than that of HAZ and base material as grain refinement enhances material strengthening. According to the Hall−Petch equation, hardness increases as the grain size decreases.

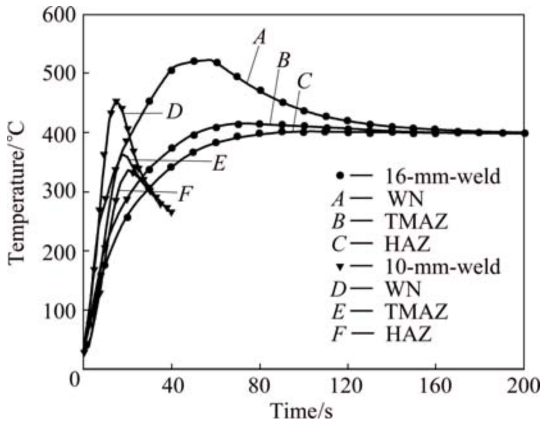

Fig. 8 Comparison of thermal cycles computed for 16-mm-welds—*A* (at the weld centre), *B* (at 15 mm from weld centre), *C* (at 18 mm from weld centre) and 10-mm-welds—*D* (at the weld centre), *E* (at 11 mm from weld centre) and *F* (at 12 mm from weld centre)

3.2.2 Tensile properties

The tensile test results of 10-mm-weld and 16-mm-weld are summarized in Table 3. Compared with unwelded base material, samples transverse to the weld show reductions in strength and elongation. The joint efficiency (based on ultimate tensile strength) of 70% was measured in 10-mm-welds and they were found to fail in 45° shear mode in HAZ of the advancing side (Fig. 9). 16-mm-welds exhibited the joint efficiency of 53% and they were also found to fracture in HAZ of the advancing side in the same mode (Fig. 10). This may be attributed to two reasons: 1) the absence of finer grains, as the grain refinement plays a key role in material strengthening in HAZ; 2) presence of wide precipitate free zones along grain boundaries and partial dissolution of precipitates in the grain interiors in the HAZ (Fig. 6(d)) which are considered to be responsible for failure. Tensile failures near HAZ of the advancing side seem to be a common feature in aluminum alloy friction stir welds, as the same was reported in several different aluminum alloys by various researchers [18,20]. Welds made on 10 mm thick plates exhibited superior tensile properties compared with those made on 16 mm thick plates though the base material properties are approximately the same. The drastic reduction in tensile properties indicates that 16-mm-weld experiences slower cooling rate (Fig. 8).

Thermal cycles were computed for both 10-mm-welds and 16-mm-welds using the model developed by SELVARAJ et al [31]. As it can be seen from Fig. 8, curves A, B and C represent thermal cycles, experienced by 16-mm-weld, in the WN, TMAZ and HAZ, respectively, and curves D, E and F represent thermal profiles, experienced by 10-mm-weld, in the WN, TMAZ and HAZ, respectively. It is evident that the welds made on 16 mm thick plates face higher peak temperatures in all three weld regions. Furthermore, 16-mm-welds experience higher temperatures for longer time which results in substantial over aging in HAZ resulting in aggravated PFZ, as shown in Fig. 6(d).

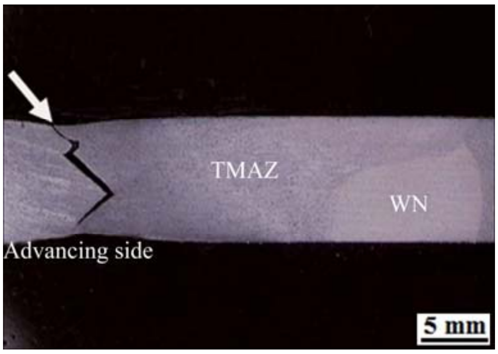

Fig. 9 Cross section of fracture surface of tensile-tested 10-mm-welds (arrow shows failure location)

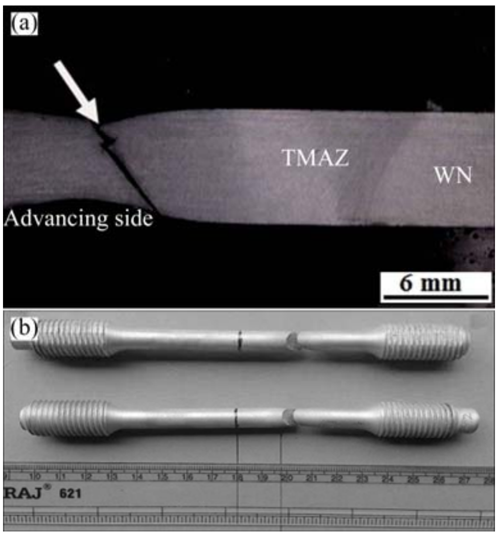

Fig. 10 Tensile-tested 16-mm-welds: (a) Cross section of fracture surface; (b) Failed specimens

3.2.3 Bend tests

In transverse face and root bend tests conducted as per ASTM E 190, 10-mm-welds were found to develop cracks at a bend angle of 50° to 60° and 10° to 15°, respectively (Fig. 11(a)). 16-mm-welds subjected to the face bend test were found to develop cracks at a bend angle of 40° to 45°, whereas in the critical root bend test, the cracks were initiated at a bend angle of 20° to 25°

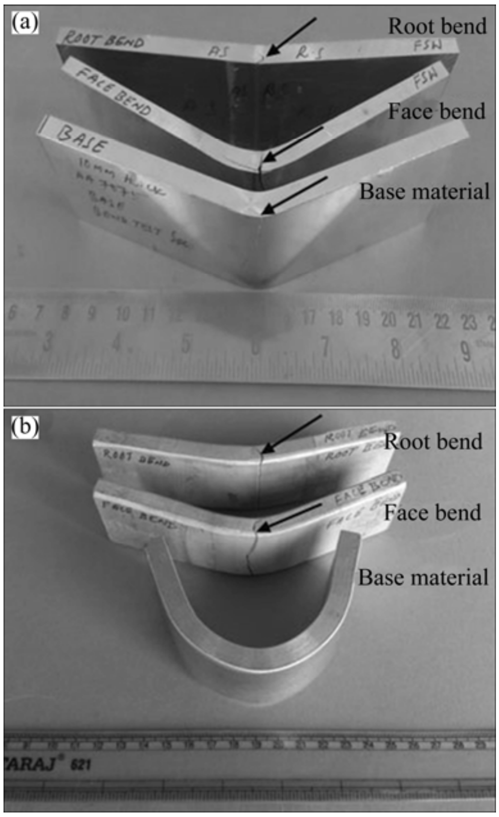

Fig. 11 Failed bend test specimens of friction stir welds: (a) 10-mm-welds; (b) 16-mm-welds (arrows showing fracture location)

(Fig. 11(b)). In comparison, the welds exhibited better resistance to transverse face bends than to critical root bends. However, bend performance of welds was found not to be satisfactory, falling far behind base material.

3.2.4 Impact toughness

Table 4 presents the impact toughness of 10-mm-welds and 16-mm-welds. It was found that the 16-mm-welds show better impact toughness compared with 10-mm-welds though the base material plates exhibit the same toughness in both 10 mm and 16 mm thicknesses. Failed impact test specimens are shown in Fig. 12.

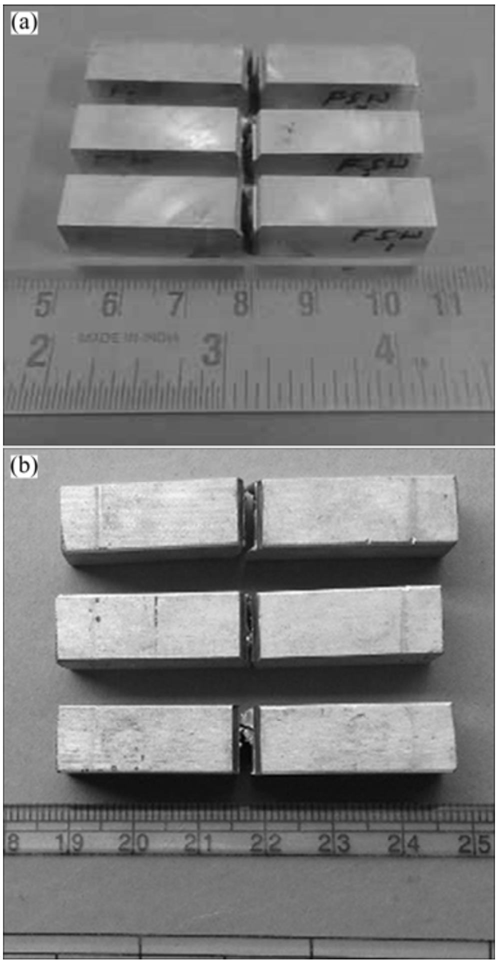

Fig. 12 Failed impact test specimens of friction stir welds: (a) 10-mm-welds; (b) 16-mm-welds

4 Conclusions

1) Defect-free friction stir welds can be easily made on 10 mm and 16 mm thick plates of AA7075−T651 alloy.

2) Significant loss in hardness occurs in the HAZ of both welds. Loss in hardness is considerably higher in the case of welds made on 16 mm thick plates, which is mainly due to the higher heat input employed to obtain sound welds. Grain refinement results in higher hardness values in the weld nugget of both the welds.

3) The joint efficiency in the case of thick plate welds is found to be only 53% for 16-mm-welds and 70% for 10-mm-welds as against the reported values of 80%−90% for 3−6 mm thick plates of the same material.

4) Welds made on 10 mm thick plates exhibit superior tensile properties compared with those made on 16 mm thick plates though the base material properties are approximately same.

5) Fracture during tensile test occurs in the HAZ area in both cases. TEM images reveal that HAZ consists of wide precipitate free zones along grain boundaries and partial dissolution of precipitates in the grain interiors, which are considered to be responsible for low tensile strength of the joints.

Acknowledgements

The authors acknowledge the financial support from Armament Research Board, DRDO, Ministry of Defence, India, through a R&D project No. ARMREB/MAA/2012/142. The authors acknowledge support extended by DMRL, Hyderabad for conducting friction stir welding trails. The authors would like to thank Mr. M. SELVARAJ, assistant professor, SSN College of Engineering, Chennai, India, for his help for computing thermal cycles.

References

[1] ABHAY K, SREEKUMAR K. Metallurgical studies on cracked Al−5.5Zn−2.5Mg−1.5Cu aluminum alloy injector disc of turbine rotor [J]. Journal of Failure Analysis and Prevention, 2008, 8(4): 327−332.

[2] ERNEST F N. Metals handbook: Welding, brazing, and soldering [M]. 9th ed. Ohio: ASM, 1983.

[3] SUA J Q, NELSON T W, STERLING C J. Microstructure evolution during FSW/FSP of high strength aluminum alloys [J]. Materials Science and Engineering A, 2005, 405: 277−286.

[4] FUJII H, CUI L, MAEDA M, NOGI K. Effect of tool shape on mechanical properties and microstructure of friction stir welded aluminum alloys [J]. Materials Science and Engineering A, 2006, 419: 25−31.

[5] CHENA Y, LIU H, FENG J. Friction stir welding characteristics of different heat-treated-state 2219 aluminum alloy plates [J]. Materials Science and Engineering A, 2006, 420: 21−25.

[6] CAVALIERE P, CAMPANILE G, PANELLA F, SQUILLACE A. Effect of welding parameters on mechanical and microstructural properties of AA6056 joints produced by friction stir welding [J]. Journal of Materials Processing Technology, 2006, 180: 263−270.

[7] CHEN H B, YAN K, LIN T, CHEN S B, JIANG C Y, ZHAO Y. The investigation of typical welding defects for 5456 aluminum alloy friction stir welds [J]. Materials Science and Engineering A, 2006, 433: 64−69.

[8] MISHRA R S, MA Z Y. Friction stir welding and processing [J]. Materials Science and Engineering R, 2005, 50: 1−78.

[9] THOMAS W M, NICHOLAS E D, NEEDHAM J C, MURCH M G, TEMPLE-SMITH P, DAWES C J. Friction Stir Butt Welding: GB Patent, 9125978.8 [P]. 1991−12−06.

[10] HASSAN K A A, PRANGNELL P B, NORMAN A F, PRICE D A, WILLIAMS S W. Effect of welding parameters on nugget zone

microstructure and properties in high strength aluminum alloy friction stir welds [J]. Science and Technology of Welding and Joining, 2003, 8: 257−268.

[11] RHODES C G, MAHONEY M W, BINGEL W H, SPURLING R A, BAMPTON C C. Effects of friction stir welding on microstructure of 7075 aluminum [J]. Scripta Materialia, 1997, 36: 69−75.

[12] JATA K V, SANKARAN K K, RUSCHAU J J. Friction-stir welding effects on microstructure and fatigue of aluminum alloy 7050-T7451 [J]. Metallurgical and Materials Transactions A, 2000, 31: 2181−2192.

[13] LIU G, MURR L E, NIOU C S, McCLURE J C, VEGA F R. Microstructural aspects of the friction-stir welding of 6061-T6 aluminum [J]. Scripta Materialia, 1997, 37: 355−361.

[14] SATO Y S, KOKAWA H, ENOMOTO M, JOGAN S, HASHIMOTO T. Precipitation sequence in friction stir weld of 6063 aluminum during aging [J]. Metallurgical and Materials Transactions A, 1999, 30: 3125−3130.

[15] SATO Y S, KOKAWA H, ENOMOTO M, JOGAN S. Microstructural evolution of 6063 aluminum during friction-stir welding [J]. Metallurgical and Materials Transactions A, 1999, 30: 2429−2437.

[16] JATA K V, SEMIATIN K L. Continuous dynamic recrystallization during friction stir welding of high strength aluminum alloys [J]. Scripta Materialia, 2000, 43: 743−749.

[17] BENAVIDES S, LI Y, MURR L E, BROWN D, McCLURE J C. Low-temperature friction-stir welding of 2024 aluminum [J]. Scripta Materialia, 1999, 41: 809−815.

[18] MAHONEY M W, RHODES C G, FLINTOFF J G, SPURLING R A, BINGEL W H. Properties of friction-stir-welded 7075 T651 aluminum [J]. Metallurgical and Materials Transactions A, 1998, 29: 1955−1964.

[19] PEEL M, STEUWER A, PREUSS M, WITHERS P J. Microstructure, mechanical properties and residual stresses as a function of welding speed in aluminum AA5083 friction stir welds [J]. Acta Materialia, 2003, 51: 4791−4801.

[20] REYNOLDS A P, LOCKWOOD W D, SEIDEL T U. Processing-property correlation in friction stir welds [J]. Materials Science Forum, 2000, 331−337: 1719−1724.

[21] LIU H J, FUJII H, MAEDA M, NOGI K. Tensile properties and fracture locations of friction-stir-welded joints of 2017–T351 aluminum alloy [J]. Journal of Materials Processing Technology, 2003, 142: 692−696.

[22] YANG B, YAN J, SUTTON M A, REYNOLDS A P. Banded microstructure in AA2024−T351 and AA2524−T351 aluminum friction stir welds: Part I. Metallurgical studies [J]. Materials Science and Engineering A, 2004, 364: 55−65.

[23] HASSAN K A A, NORMAN A F, PRANGNELL P B. The stability of the nugget zone grain structure in AA7010 alloy friction stir welds during solution treatment [J]. Materials Science Forum, 2002, 396−402: 1549−1554.

[24] HASSAN K A A, NORMAN A F, PRANGNELL P B. The effect of welding conditions on the microstructure and mechanical properties of the nugget zone in AA7010 alloy friction stir welds [C]//Proceedings of the Third International Symposium on Friction Stir Welding. Kobe, Japan: 2001.

[25] JATA K V. Friction stir welding of high strength aluminum alloys [J]. Materials Science Forum, 2000, 331−337: 1701−1712.

[26] ROBSON J D, SULLIVAN A, SHERCLIFF H R, McSHANE G. Microstructural evolution during friction stir welding of AA7449 [C]//Proceedings of the Fifth International Symposium on Friction Stir Welding. Metz, France, 2004.

[27] PRIME M B, GNÄUPEL-HEROLD T, BAUMANN J A, LEDERICH R J, BOWDEN D M, SEBRING R J. Residual stress measurements in a thick, dissimilar aluminum alloy friction stir weld [J]. Acta Materialia, 2006, 54: 4013−4021.

[28] RAJKUMAR S, MURALIDHARAN C, BALASUBRAMANIAN V. Influence of friction stir welding process and tool parameters on strength properties of AA7075–T6 aluminum alloys joints [J]. Materials and Design, 2011, 32: 535−549.

[29] WERT J A. Identification of precipitates in 7075 Al after high-temperature aging [J]. Scripta Materialia, 1981, 15: 445−447.

[30] LORIMER G W. Precipitation in aluminum alloys [C]//RUSSELL K C, AARONSON H I, eds. Precipitation processes in Solids. Warrendale, PA: TMS-AIME, 1978: 87−119.

[31] SELVARAJ M, MURALI V, KOTESWARA RAO S R. Mechanism of weld formation during friction stir welding of aluminum alloy [J]. Materials and Manufacturing Processes, 2013, 28: 595−600.

搅拌摩擦焊 AA7075-T651 铝合金厚板的显微组织和力学性能

T. SRINIVASA RAO[1], G. MADHUSUDHAN REDDY[2], S. R. KOTESWARA RAO[3]

1. Department of Mechanical Engineering, Tagore Engineering College, Chennai 600127, Tamil Nadu, India;
2. Metal Joining Group, Defense Metallurgical Research Laboratory, Hyderabad 500058, Telangana, India;
3. Department of Mechanical Engineering, SSN College of Engineering, Kalavakkam 603110, Tamil Nadu, India

摘　要：研究厚度为 10 和 16 mm AA7075-T651 板的搅拌摩擦焊接过程。通过仔细选择焊接过程参数可获得无缺陷、全渗透焊接样品。两种焊接接头都出现极细的再结晶晶粒，而 10 mm 厚板焊接接头的晶粒组织更细。试样的显微组织观察结果表明，焊件热影响区的硬度显著降低。16 mm 厚合金板焊接接头的硬度降低较大。与 16 mm 厚合金板相比，10 mm 厚合金板焊件具有较优的拉伸性能。在拉伸实验过程中，两种厚度的合金板焊件均在热影响区发生断裂。样品的 TEM 结果表明，热影响区由沿晶界的宽化无沉积区和晶体内沉淀的部分溶解组成。因此，采用搅拌摩擦焊在 AA7075-T651 上可制得单道次无缺陷焊件，且 10 mm 厚合金板焊件表现出较高的焊接效率。

关键词：AA7075-T651 铝合金；搅拌摩擦焊；显微组织；力学性能

(Edited by Wei-ping CHEN)